Global reorganization of budding yeast chromosome conformation in different physiological conditions

Elisa Dultz,[1,2] Harianto Tjong,[3] Elodie Weider,[1] Mareike Herzog,[1] Barry Young,[5] Christiane Brune,[1] Daniel Müllner,[4] Christopher Loewen,[5] Frank Alber,[3] and Karsten Weis[1,2]

[1]Department of Molecular and Cell Biology, University of California, Berkeley, Berkeley, CA 94720
[2]Department of Biology, Institute of Biochemistry, Eidgenössische Technische Hochschule Zurich, 8093 Zurich, Switzerland
[3]Department of Biological Sciences, Molecular and Computational Biology, University of Southern California, Los Angeles, CA 90089
[4]Department of Mathematics, Stanford University, Stanford, CA 94305
[5]Department of Cellular and Physiological Sciences, Life Sciences Institute, University of British Columbia, Vancouver, BC V6T1Z3, Canada

The organization of the genome is nonrandom and important for correct function. Specifically, the nuclear envelope plays a critical role in gene regulation. It generally constitutes a repressive environment, but several genes, including the *GAL* locus in budding yeast, are recruited to the nuclear periphery on activation. Here, we combine imaging and computational modeling to ask how the association of a single gene locus with the nuclear envelope influences the surrounding chromosome architecture. Systematic analysis of an entire yeast chromosome establishes that peripheral recruitment of the *GAL* locus is part of a large-scale rearrangement that shifts many chromosomal regions closer to the nuclear envelope. This process is likely caused by the presence of several independent anchoring points. To identify novel factors required for peripheral anchoring, we performed a genome-wide screen and demonstrated that the histone acetyltransferase SAGA and the activity of histone deacetylases are needed for this extensive gene recruitment to the nuclear periphery.

Introduction

The genome is highly organized within the eukaryotic cell nucleus, and different functional domains and territories can be identified (Bickmore and van Steensel, 2013; Pombo and Dillon, 2015). Nevertheless, recent modeling results indicate that the global conformation of the yeast genome is largely governed by simple physical rules (Tjong et al., 2012; Wong et al., 2012). Using a small number of physical restraints, e.g., the tethering of centromeres to the spindle pole body and telomeres to the periphery, these models reproduce experimental results with very good accuracy. This suggests that specific interactions with chromatin binding factors are not required to maintain the global chromatin conformation observed in exponentially growing budding yeast cells. Similarly, experimental data gained by analyzing nuclear positioning and dynamics of several loci along chromosome XII can be interpreted with physical models considering constraints of a tethered polymer and volume exclusion (Albert et al., 2013).

However, the specific localization of genes within the nucleus can change dramatically in response to stimuli. For example, certain budding yeast genes associate with the nuclear periphery specifically when they are actively transcribed (Brickner and Walter, 2004; Casolari et al., 2004; Taddei et al., 2006), suggesting that local changes in genome organization occur in a regulated manner.

The budding yeast *GAL* locus on chromosome II (chr II) is a well-studied model locus in this context. It consists of three genes, *GAL7*, *GAL10*, and *GAL1*, which encode enzymes involved in galactose metabolism. The locus is strongly repressed in the presence of glucose by the glucose repression pathway via the transcriptional repressor Mig1 (Johnston, 1999) and is directly activated by the hexose galactose (Bash and Lohr, 2001). The *GAL* locus was first shown by fluorescence in situ hybridization to relocalize from a random position within the nucleus to the nuclear periphery on activation, and this was accompanied by the association of the locus with nuclear pore components by chromatin immunoprecipitation (Casolari et al., 2004). Nuclear envelope recruitment has been reported to depend on the presence of promoter sequences for the *GAL2* gene (Dieppois et al., 2006) and to be influenced by the 3′ UTR for a reporter gene construct based on *GAL1* (Abruzzi et al., 2006). Furthermore, factors of the transcriptional activation machinery, the mRNA processing and export machinery, and the nuclear pore complex (NPC) are required to establish peripheral localization (Cabal et al., 2006; Dieppois et al., 2006; Vodala et al.,

Correspondence to Elisa Dultz: elisa.dultz@bc.biol.ethz.ch

Abbreviations used in this paper: chr II, chromosome II; HAT, histone acetyltransferase; HDAC, histone deacetylase; NPC, nuclear pore complex; SGA, synthetic genetic array; TSA, trichostatin A.

The Rockefeller University Press $30.00
J. Cell Biol. Vol. 212 No. 3 321–334
www.jcb.org/cgi/doi/10.1083/jcb.201507069

2008). Interestingly, recent work has shown that the *GAL* locus is found at the nuclear periphery not only in activating conditions (galactose) but also in cells growing in raffinose (Green et al., 2012), where the *GAL* genes are off although repression through Mig1 has been relieved (Johnston, 1999).

Therefore, the position of individual loci within the nucleus can be differentially regulated depending on physiologic conditions. How such a local regulation influences surrounding regions that are connected on a linear chromosome is unknown. Is the peripheral recruitment restricted to short chromosomal loops? Are larger areas of chromosomes affected? What are the functional consequences of this gene movement? This is especially relevant in an organism like *Saccharomyces cerevisiae* that has a relatively small genome with high gene density and short chromosomes that have been suggested to behave like stiff rods (Therizols et al., 2010).

In this study, we examined how tethering of the *GAL* locus to the nuclear periphery influences the localization of neighboring genes and further characterized the mechanism of this gene recruitment to the nuclear periphery. We developed an automated imaging pipeline and combined it with modeling to demonstrate that changes in association with the periphery in galactose-growing cells are not unique to the *GAL* locus but extend to large parts of the entire chromosome, likely because of the presence of multiple chromosomal tethering sites. In addition, we used our automated imaging platform to perform a genome-wide screen, which revealed that peripheral tethering requires both acetylation and deacetylation activities.

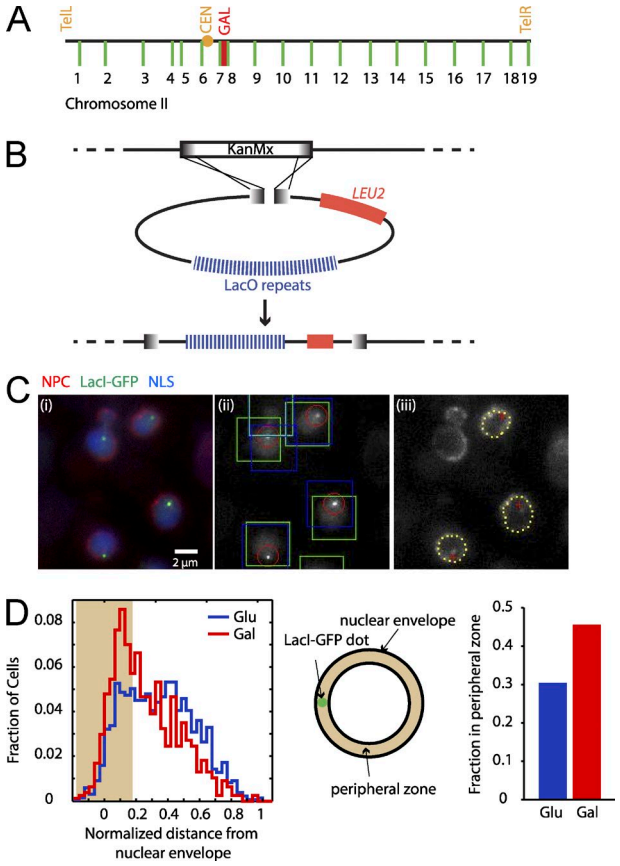

Figure 1. **Overview of strain construction and image analysis.** (A) Schematic representation of *S. cerevisiae* chr II with LacO repeat integration sites in the different strains indicated in green. The location of the centromere (CEN), the *GAL7-GAL10-GAL1* locus (GAL), and the telomeres (TEL) are indicated. (B) Schematic representation of insertion scheme for LacO repeats using strains from the genome deletion collection. (C) Overview of image analysis pipeline. (i) shows an example image of yeast cells carrying LacO repeats inserted at a genomic locus and expressing the fluorescent markers RPL25NLS-CFP, Ndc1-tdTomato, and LacI-GFP; (ii) shows fluorescence from the LacI-GFP channel and marks objects detected by the analysis code (red circle: gene dot; green box: cell nucleus by RPL25NLS-CFP; blue box: NPC signal); (iii) shows final cells analyzed (red cross: gene dot; yellow dotted line: nuclear envelope trace). (D) Example for histogram of distance distribution in population of cells grown either in glucose (Glu) or galactose (Gal). Shaded area indicates cutoff used to generate bar graph (right). The peripheral zone encompasses one third of the area of the nuclear cross section.

Results

Construction of the chr II strain library

Several individual gene loci in yeast have been observed to relocate toward the nuclear periphery on transcriptional activation (Brickner and Walter, 2004; Casolari et al., 2004; Taddei et al., 2006). To study how such changes in the localization of individual loci impact surrounding chromosome regions or entire chromosomes, we designed a library of strains which carry LacO repeats (that can be visualized with LacI tagged with GFP) at equally spaced positions along the entire yeast chr II (Fig. 1 A), which harbors the *GAL* gene cluster. To facilitate generation of this strain library, we used a LacO repeat containing plasmid designed to replace the KanMX cassette in strains of the yeast genome deletion collection (Fig. 1 B; Winzeler et al., 1999; Rohner et al., 2008). With this strategy we generated integrations spaced approximately every 50 kb along chr II. In addition, we introduced fluorescent markers for the nucleoplasm (NLS of Rpl25 tagged with CFP) and the nuclear envelope (nucleoporin Ndc1 tagged with tdTomato).

For unbiased analysis of large numbers of cells in different stains and conditions, we developed an automated imaging and image analysis pipeline based on wide-field epifluorescence microscopy and dedicated MATLAB code. The nucleoplasmic NLS marker facilitated segmentation, whereas the nucleoporin allowed tracing of the nuclear periphery (Fig. 1 C). After initially fitting an ellipse to the nuclear pore signal, the tracing of the nuclear envelope was refined using free-form and spline fitting (see Materials and methods for details). Importantly, our method does not enforce circular or ellipsoid shapes. The minimal distance between the gene dot and the nuclear envelope was analyzed for each cell and normalized to the nuclear radius. Gene dots in a peripheral zone encompassing one third of the cross-sectional area of the nucleus were classified as peripheral (Fig. 1 D). As expected, in a strain marked with LacO repeats next to the *GAL* locus, the distribution of distances between the gene and nuclear envelope shifted from a broad distribution over the entire width of the nuclear radius to a strongly skewed distribution peaking close to the nuclear envelope on growth in galactose (Fig. 1 D). Our automated analysis method performed quantitatively very similar to previously published manual analysis methods (Fig. S1 A; Dieppois et al., 2006). Furthermore, this approach can be easily adapted for the analysis of 3D information if higher accuracy is desired (Fig. S1 B). Therefore, our automated imaging pipeline provided us with a robust platform to rapidly acquire and analyze gene localization in a large number of cells in different growth conditions.

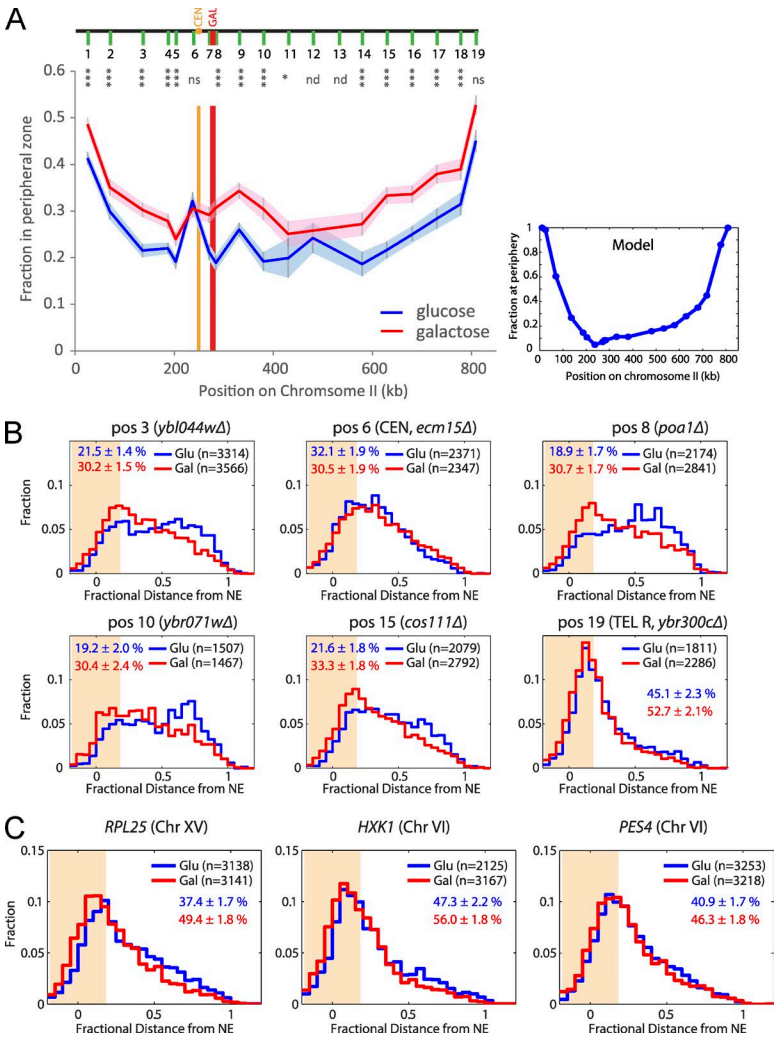

Figure 2. **Global changes in chromosome localization in galactose.** (A) Fraction of cells with peripheral gene dots in cells grown in either glucose (blue) or galactose (red). Shaded areas indicate 95% confidence intervals. ***, $P < 0.001$; *, $P < 0.01$; ns, not significant ($P > 0.01$) for *z* test of proportions; nd, not determined. Data are pooled from at least four biological replicates for each strain with typically 200–400 individual cells analyzed each (minimum of 80). Small plot on right shows gene localization obtained from computational model as in Tjong et al. (2012) with cutoff for peripheral zone at 183.5 nm. (B and C) Histograms of distances for indicated positions on chr II (B) and for loci on other chromosomes (C; additional loci see Fig. S2, A and B). Percentage of cells in peripheral zone are indicated in blue (glucose [Glu]) and red (galactose [Gal]). *n* = number of cells analyzed; pos, position.

Chromosome localization relative to the nuclear envelope in glucose and galactose

First, we analyzed the localization of chr II loci relative to the nuclear envelope in exponentially growing cells using glucose as their carbon source. The telomeres and centromere localized to the nuclear periphery at the highest percentage, as expected (Fig. 2 A, blue). Loci in between were located further away, with a gradual shift from the telomeres toward the center of the chromosome arm and a rather abrupt drop of peripheral localization at positions surrounding the centromere. The latter effect is likely caused by crowding in the area around the spindle pole body (Tjong et al., 2012). These observations are also reflected in histograms of the distribution of distances, displaying narrow peaks close to the nuclear periphery for the tethered sites at the telomeres and centromere and broader more symmetric distributions for sites in the center of the chromosome arms (Figs. 2 B and S2 A).

We recently developed a computational model for the conformation of the yeast genome using few biophysical constraints and a priori assumptions (Tjong et al., 2012). Our model showed very high correlation with experimental data obtained by live-cell imaging and chromatin conformation capture techniques (Tjong et al., 2012). Consistent with this, the overall features that we observed here for chr II were recapitulated in our computational model (Fig. 2 A, right). Two discrepancies became apparent. First, in the model, the centromere was not closer to the nuclear periphery than neighboring loci. The centromere localization in the model was based on previous experimental observations (Jin et al., 2000; Berger et al., 2008; Therizols et al., 2010). The difference might be explained if the yeast strain used in our current study had shorter microtubules. Alternatively, the labeling of Ndc1, which also is a component of the spindle pole body, may have improved detection of the nuclear envelope in the area of the spindle pole body and therefore more precisely localized the centromere close to it. A second difference concerns the localization of telomeres. In the computational model, 100% of telomeres were kept in a narrow zone at the nuclear envelope. However, in previous experiments, only 50–70% of different telomeres were scored as peripheral in different cell cycle phases (Hediger et al., 2002b), and we found 41.4 ± 1.4% (95% confidence interval, position 1) for the left telomere and 45.1 ± 2.3% (position 19) for the right telomere within the peripheral zone of the nuclear envelope.

Next, we analyzed how the positioning of chr II changed on induction of the *GAL* genes. As expected (Green et al., 2012), a gene tag in the vicinity of the *GAL* locus (5 kb telomeric of the *GAL* locus, position 8) localizes to the peripheral zone in a higher percentage of cells in galactose when compared with glucose-grown cells (30.7 ± 1.7% vs. 18.9 ± 1.7%). The loci surrounding the *GAL* locus (positions 7–10) also showed increased peripheral localization in galactose-growing cells, but the centromere (position 6) was not affected. To our surprise,

this peripheralization effect was not restricted to the neighborhood of the *GAL* locus: also gene loci positioned far away on chr II showed increased localization to the nuclear periphery. A notable exception was position 11, which did not show a strong change in localization between glucose and galactose (Fig. 2 A; compare also Fig. 5 B). These results suggest that the association of the *GAL* locus with the nuclear periphery is not a singular event but is part of a large-scale rearrangement affecting the entire chr II.

To assess whether this phenomenon was restricted to chr II, we analyzed the localization of additional genes on other chromosomes. In agreement with previous results (Taddei et al., 2006), we found that the telomere proximal and glucose repressed *HXK1* gene on chromosome VI also shows slightly increased localization at the nuclear periphery in galactose; however, this was not true for *PES4* (also on chromosome VI; Fig. 2 C). However, several other genes, which are not implicated in carbon metabolism, including *RPL25* (chromosome XV), *RPL9A* (chromosome VII), and *INO1* (chromosome X), also associated with the nuclear envelope in a larger percentage of cells in galactose- compared with glucose-grown cells (Figs. 2 C and S2 B). Therefore, the shift toward the nuclear envelope is not unique to chr II. Rather, it seems to be a large-scale chromosome rearrangement caused by changes in the gene expression program or physiological state of the cell when grown in galactose compared with glucose.

Although it appeared unlikely that the *GAL* locus alone would be responsible for the observed large-scale chromosome rearrangement in galactose-growing cells, we used our computational model to examine the effects of a single tethering site on chromosomal organization. To this end, we forced the *GAL* locus to be localized 50 nm from the nuclear periphery (tethered) in 40% of our model population. In this model, localization of a region extending ∼100 kb in each direction from the *GAL* locus shifts toward the nuclear periphery (Fig. 3 A and see Fig. S3 A for a model with 100% *GAL* loci tethered). However, regions that were further away in linear chromosome distance were only moderately affected in the model (e.g., on the right arm from position 12 on).

We next tested this model experimentally by introducing a single artificial tether on chr II. Expression of a TetR-tagged nucleoporin (Mlp1) in a strain that also contained TetO repeats proximal to the *GAL* locus led to the peripheral recruitment of this locus in glucose-grown cells (Fig. 3 B). Similar to our computational model, peripheral regions of up to 100 kb were affected by this artificial tether, but no effect could be observed beyond this distance. Therefore, tethering of a single gene locus can significantly influence the nuclear positions of surrounding genes up to ∼100 kb. However, additional factors must contribute to the large-scale changes observed in galactose-grown cells.

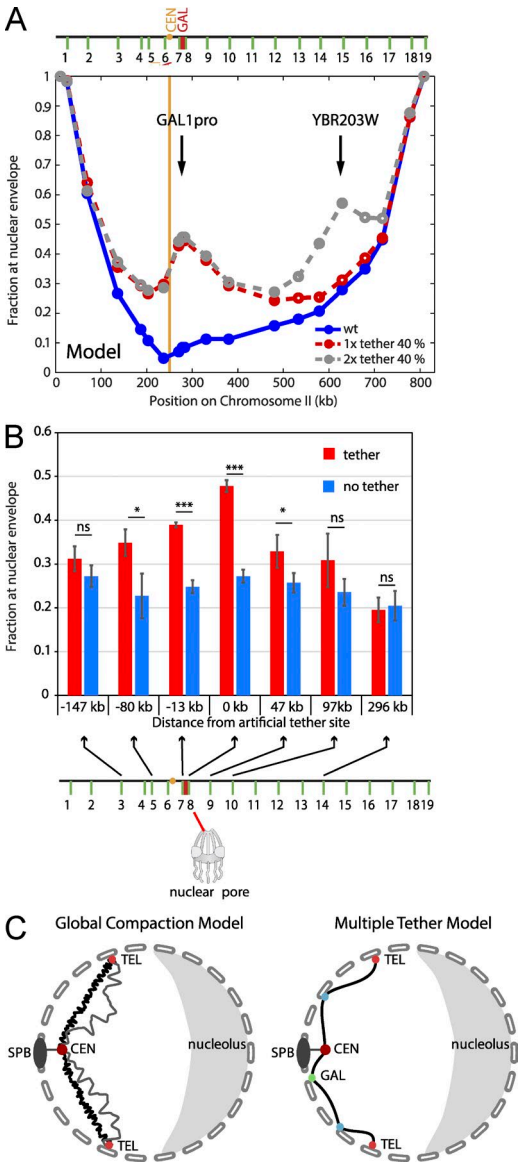

Figure 3. **A single tether has local effects only.** (A) Computational model of chr II conformation. Fraction of loci localized in peripheral zone (<183.5 nm from nuclear periphery) in a wild-type (wt) model (blue) and in models where either the *GAL1* promoter (dashed red) or the *GAL1* promoter and the *YBR203W* locus (dashed gray) are tethered to the nuclear envelope in 40% of nuclei. (B) Fraction of loci localized in peripheral zone in strains with TetO repeats close the *GAL* locus tethered to the nuclear pore by Mlp1-TetR (red) or wild-type strains (blue). Bars show mean of three experiments (>70 cells each). Error bars show SD. Asterisks indicate significance level of an unpaired two-tailed *t* test (*, $P < 0.05$; ***, $P < 0.001$; not significant [ns], $P > 0.05$). (C) Models for achieving peripheralization of a chromosome in budding yeast. SPB, spindle pole body; TEL, telomere; CEN, centromere.

Can global compaction explain peripheralization of chr II in galactose?

What mechanism could trigger this chromatin rearrangement? We considered two—not mutually exclusive—hypotheses. First, because yeast cells grow slower in galactose, we hypothesized that global down-regulation of gene expression might lead to condensation of chromatin. Because yeast chromosomes are anchored at the nuclear envelope, compaction of chromatin between anchoring points could then potentially bring the chromosome closer to the nuclear envelope (Fig. 3 C, left). Alternatively, multiple tethering points on chr II and other chromosomes could be activated in galactose-growing cells, which would lead to the recruitment of multiple segments of the genome to the nuclear envelope (Fig. 3 C, right).

In our computational model, at least a 1.8-fold compaction was needed to cause a detectable increase of peripherally localized loci (Fig. S3 B). Such a compaction would lead to an estimated reduction of the mean 3D distance between two loci on the same chromosome arm by 16–19% (Fig. S3 C). We therefore tested the global compaction model experimentally by

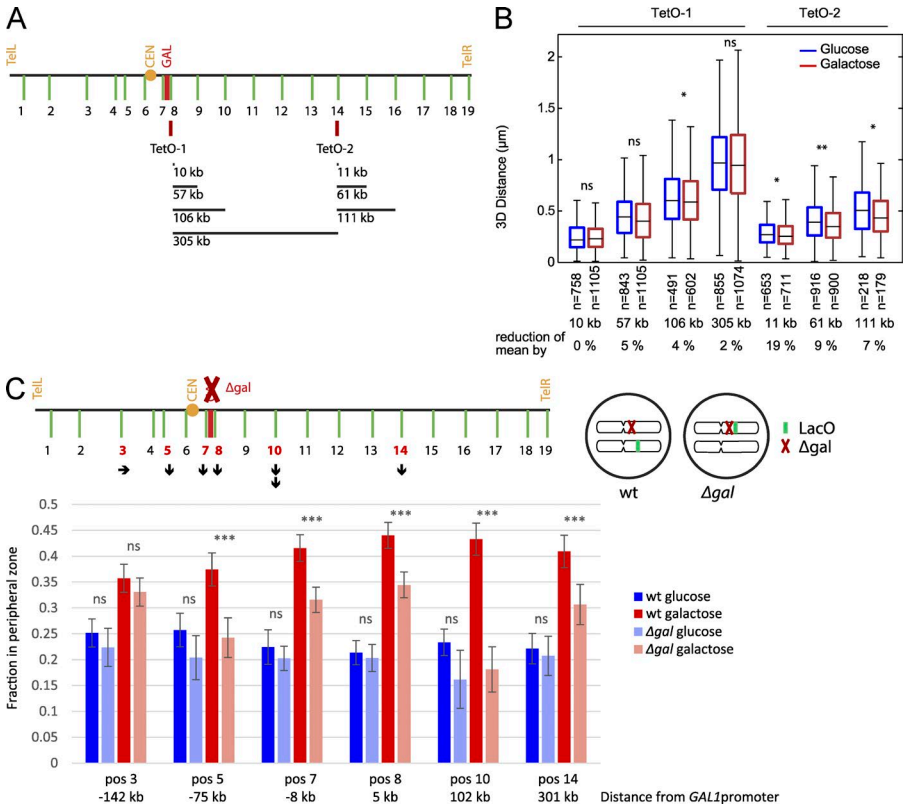

Figure 4. **Global compaction or multiple tethers?** (A) Schematic representation of pairs of loci 10–300 kb apart on chr II analyzed for 3D distance in B. (B) Boxplots of 3D distances for each pair of loci measured in cells grown in either glucose or galactose. Black line indicates median, box shows 25–75 percentile, and whiskers are to 5 and 95%. Significances from a Mann Whitney test are indicated: not significant (ns), $P > 0.05$; *, $P < 0.05$; **, $P < 0.01$. (C) Fraction of loci localized in peripheral zone in diploid cells carrying a wild-type (wt) or *Δgal* version of the *GAL* locus on the marked chromosome. Data are pooled from three to four biological replicates (>50 cells each). Error bars indicate 95% confidence intervals. ***, $P < 0.001$ for two-proportions *z* test; ns, not significant ($P > 0.05$).

introducing two fluorescent marks into chr II at different linear distances to each other (~10–305 kb; Fig. 4 A) and analyzed the 3D distance between these marks in different growth conditions. Only much smaller differences in the 3D distances for any of the pairs of markers could be detected in galactose- versus glucose-grown cells (Fig. 4 B). Therefore, global compaction alone cannot explain the observed large-scale chromatin rearrangements in galactose. Nevertheless, it cannot be excluded that slight compaction in conjunction with other mechanisms might contribute to peripheralization of chromatin in galactose-grown cells.

How does the *GAL* locus contribute to chr II rearrangement?

Our alternative hypothesis proposes the presence of multiple tethers in galactose-growing cells. If this was true, removal of the *GAL* locus (the only identified tethering site on chr II) would be expected to have local effects on its genomic neighborhood but would not abolish localization changes further away. We examined the localization of several loci on chr II after deletion of *GAL7*, *GAL10*, and *GAL1*, including upstream and downstream sequences (*Δgal*). To allow for growth in galactose medium, these experiments were performed in diploid cells containing a second unmarked copy of chr II (Fig. 4 C). Like in haploid strains, peripheral recruitment of loci along the entire chr II was observed in galactose growing diploid cells (Fig. 4 C). As expected, the percentage of cells in which the chromosome region surrounding the *GAL* locus was localized at the nuclear periphery was significantly reduced in *Δgal* strains. However, there still was an increase in peripheral localization in galactose compared with glucose, suggesting that even in the immediate vicinity of the *GAL* locus additional anchor points might exist. In line with a multiple tether model, a locus on the left arm of chr II and 140 kb away from the *GAL* locus (position 3) was not affected. Surprisingly, the gene locus at position 14, 300 kb away on the right arm of chr II, still showed a significant reduction in the fraction of cells with peripheral localization in galactose. Therefore, although individual anchoring points might influence each other over large distances, overall our results are consistent with a multiple tether model.

How many tethering sites exist?

To approach the question of how many tethering sites are needed to generate the experimentally observed localization pattern, we again explored our computational model. The introduction of one additional tethering site at position 15 on the right arm of chr II led to an increase in peripheral localization of a chromosome region of ~100 kb in each direction (Fig. 3 A, gray), indicating that the presence of very few distinct tethering sites on chr II could generate the observed large-scale changes in localization. We therefore hypothesize that in addition to the *GAL* locus, there is at least one additional tethering site on the right arm of chr II. Alternatively, multiple weaker tethering sites could generate a similar effect.

Apart from the three genes at the *GAL* locus, no other genes on chr II are strongly induced specifically in galactose (Gasch and Werner-Washburne, 2002). However, growth in galactose also leads to increased expression of a large number of glucose-repressed genes, and we therefore wanted to test whether the withdrawal of glucose rather than the addition of galactose was the driving force behind the observed changes in localization. We analyzed the localization of chr II in cells growing in raffinose, a condition in which glucose repression is relieved, but the *GAL* genes are not activated. As previously reported, the *GAL* locus localized at the nuclear periphery also in raffinose (Fig. 5 A; Green et al., 2012). In addition, the peripheral

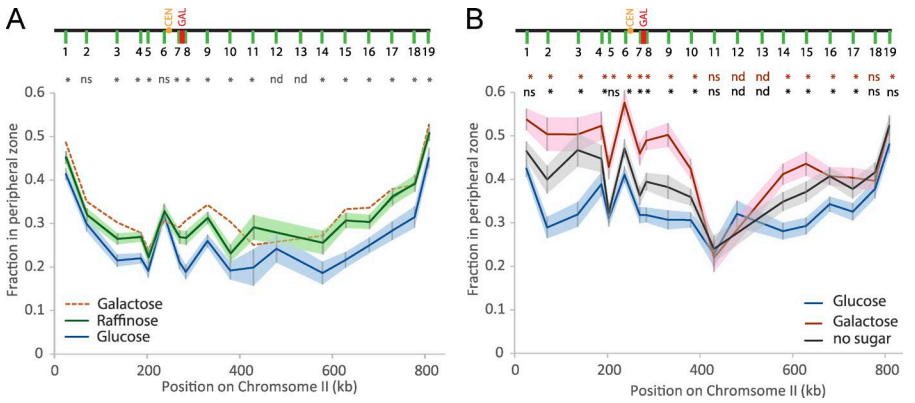

Figure 5. **Glucose deprivation leads to peripheralization.** (A) Fraction of cells with peripheral gene dots in cells grown in the indicated carbon sources. Shaded areas indicate 95% confidence intervals. Galactose data are shown as dashed line for comparison (as in Fig. 2). (B) Fraction of cells with peripheral gene dots in cells acutely washed from exponential growth in glucose to media containing either no sugar, 2% galactose, or 2% glucose (after two washed with sugar-free medium). Measurements were taken 30–60 min after carbon source shift. (A and B) Data are pooled from three to four biological replicates (>50 cells each). Shaded areas show 95% confidence intervals. *, P < 0.01; ns, not significant (P > 0.01); nd, not determined for two-proportions *z* test (for B: glucose and galactose in red or glucose and no sugar in black).

localization of chr II was overall very similar in exponentially growing cells in raffinose and galactose (Fig. 5 A). A similar effect with even stronger pronounced peripheral localization was observed in cells that were acutely washed from glucose to either sugar-free or galactose-containing medium (Fig. 5 B). Note that the peripheral levels in cells washed back into glucose are still increased 1 h after the wash compared with exponentially growing cells (compare blue lines in Fig. 5, A and B). Collectively, these observations support the hypothesis that the absence of glucose is sufficient for formation of the postulated tethering sites and the observed global chromatin reorganization.

Genome-wide screen reveals role of histone deacetylases in chromatin peripheralization

Because our results pointed to the existence of additional peripheral anchor points, we next wanted to explore the mechanism underlying the formation of these tethers. The mechanism tethering the *GAL* locus to the nuclear periphery has been postulated to be a link between the transcriptional activator complex SAGA, the nuclear export machinery, and the NPC (Rodríguez-Navarro et al., 2004; Cabal et al., 2006; Luthra et al., 2007; Jani et al., 2014). However, several pieces of conflicting data in the literature prompted us to reinvestigate the requirements of *GAL* locus relocalization to the nuclear periphery in an unbiased manner. We took advantage of our automated microscopy and image analysis pipeline to perform a genome-wide screen to identify novel factors involved in gene tethering at the nuclear periphery. We analyzed the localization of the *GAL* locus in galactose-grown strains derived from the yeast deletion collection each carrying 1 of 4,792 unique, nonessential ORF deletions. Among the 114 top hits showing reduced peripheral localization in galactose in two biological replicates of the screen, we found several chromatin modifiers (Fig. 6 A and see Table S4 for full screening results). Interestingly, among those were members of two distinct histone deacetylase (HDAC) complexes in yeast (*SIN3*, *SET3*, *UME6*, *RXT2*, and *DEP1*). Set3 and the HDACs Hos2 and Hst1 form the Set3 complex (Pijnappel et al., 2001). *SIN3*, *UME6*, *RXT2*, and *DEP1* code for members of the Rpd3 HDAC complex (Yang and Seto, 2008). In addition, *HDA1*, which encodes the HDAC in the eponymous Hda1 complex (Yang and Seto, 2008), also ranked highly (rank 137). Independently generated *hda1Δ* and *rpd3Δ* mutants recapitulated the relocalization defect (Fig. 6 B). Both mutants reduced association of the *GAL* locus with the nuclear periphery in galactose but also in glucose, suggesting that any residual tethering in glucose is also affected. We also deleted *RCO1* and *SDS3*, which are components of the two flavors of the Rpd3 complex, namely Rpd3L and Rpd3S (Yang and Seto, 2008). Although the localization pattern in the *rco1Δ* strain closely resembled localization in the *rpd3Δ* mutant, deletion of *SDS3* affected only localization in galactose, but it did not show a reduction in peripheral localization of the *GAL* locus in cells growing in glucose, suggesting that the two complexes may play distinct roles. Importantly, treatment with the HDAC inhibitor trichostatin A (TSA), which targets both Rpd3 and Hda1, recapitulated the reduction of peripheral localization of the *GAL* locus observed in the HDAC mutants (Fig. 6 C).

It was previously shown that chromatin association with the nuclear periphery is regulated throughout the cell cycle (Hediger et al., 2002b; Brickner and Brickner, 2010). Although we did not find an enrichment of cell cycle regulators among our hits, we investigated whether changes in cell cycle distribution on TSA treatment or in HDAC-mutant cells could indirectly contribute to reduced peripheral association. However, neither the treatment with TSA nor the loss of *HDA1* or *SDS3* affected cell cycle distribution in the cell population (Fig. S4, C and E). Of note, *rpd3Δ* and *rco1Δ* cells displayed defects in cell cycle distributions, and the results from these mutants should therefore be interpreted with caution. Importantly, the HDAC mutants or TSA treatment did not abolish the transcriptional induction of the *GAL* or glucose-repressed genes (Fig. S4, A, B, and D). However, we observed a moderate increase in expression of both glucose-repressed and galactose-induced genes in all TSA-treated samples, consistent with a generally repressive role of histone deacetylation.

Having established that the effects of HDAC inhibition cannot be explained by changes in cell cycle distribution or inhibition of transcription, we next tested whether HDAC activity is needed for the large-scale chromatin rearrangement that we had observed. To this end, we examined our chr II strain library on treatment with TSA. The presence of TSA completely prevented peripheralization of the chromosome during growth in galactose (Fig. 7). Interestingly, we also observed that the locus next to the centromere (position 6) showed reduced localization at the nuclear periphery in the presence of TSA in both glucose and galactose. This suggests that the stable attachment of the centromere to the spindle pole body or the length of the connecting microtubules may be regulated by HDAC activity. The change in centromere localization might have a longer range

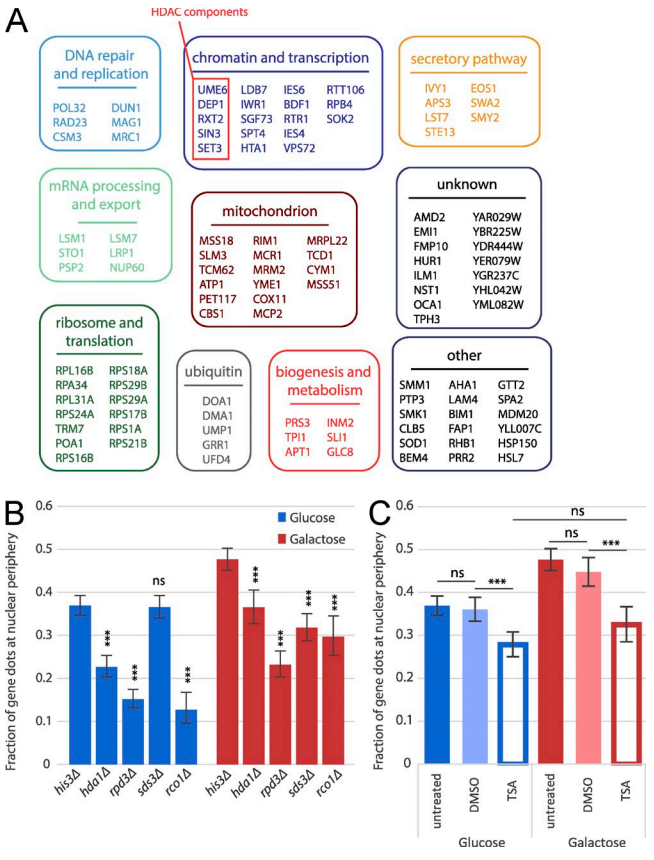

Figure 6. **Genome-wide screen identifies role of HDACs in *GAL* tethering.** (A) Classification of top hits in screen for *GAL* locus tethering mutants. Genes were manually assigned to groups according to gene ontology terms and description in the Saccharomyces Genome Database. Hits assigned as "dubious" were omitted ($n = 4$). (B) Localization of the *GAL* locus was determined in mutants for HDAC components in glucose and galactose. *his3Δ* mutant served as control. (C) Localization of the *GAL* locus was determined in the *his3Δ* mutants in presence or absence of TSA. (B and C) Data shown are pooled from three independent experiments (>50 cells each), error bars show 95% confidence intervals. ***, $P < 0.001$ for two-proportions *z* test; ns, not significant ($P > 0.01$).

effect on chromosome organization and could therefore be partially responsible for the reduced peripheral localization we observe in TSA-treated cells grown in galactose. However, we have shown that individual tethering sites affect no more than 100 kb in each direction (Fig. 3 B), rendering such a global effect unlikely. In addition, the localization in glucose is changed only locally at the centromere.

SAGA and NPCs play global roles in chromatin peripheralization

The transcriptional activator SAGA is required for targeting of the *GAL* locus to the nuclear periphery (Cabal et al., 2006). Although SAGA's histone acetyltransferase (HAT) activity had previously been suggested to be dispensable for this (Cabal et al., 2009), its HAT activity is required for anchoring DNA circles to the NPC (Denoth-Lippuner et al., 2014). Therefore, we reinvestigated the role of SAGA's enzymatic activities as HAT (via Gcn5) or deubiquitinylase (via Ubp8) in the localization of chr II. Although a shift toward the periphery could still be observed locally around the *GAL* locus in the *gcn5Δ* strain, overall both *ada2Δ* and *gcn5Δ* cells showed a very similar reduction in the association with the periphery in galactose along the length of chr II (Fig. 8, A–C), suggesting that acetylation plays a critical role in global chromosome relocalization.

In contrast, the deletion of components of SAGA's deubiquitination module, Sgf73 and Ubp8, had only moderate effects on global chromosome localization in galactose-growing cells (Fig. 8, D and E). However, *sgf73Δ* cells showed a local reduction in peripheral localization around the *GAL* locus, consistent with the fact that *SGF73* was among the top scoring genes in our genome-wide screen (Fig. 6 A and Table S4) and previous findings (Köhler et al., 2008).

Components of the NPC, including Nup60, Nup1, and Mlp1/2, have also been implicated in tethering active genes to the nuclear periphery (Cabal et al., 2006; Dieppois et al., 2006; Ahmed et al., 2010). *NUP60*, which is thought to anchor the nuclear basket proteins Mlp1 and Mlp2 to the NPC (Feuerbach et al., 2002), was found among the top genes in our screen (Fig. 6 A and Table S4). To examine the role of the NPC in general chr II localization, we deleted *NUP60* in our library strains. Although *nup60Δ* cells displayed reduced levels of peripheralization along the entire right arm of chr II, an increase in the localization at the periphery in galactose compared with glucose could still be detected (Fig. 8 F).

Interestingly, in SAGA mutants and in *nup60Δ* mutants, the peripheral localization of the telomeres, especially the left telomere, was also reduced. In some cases, loss of the telomere from the periphery was partially rescued in galactose.

In summary, our results confirm previously identified functions of the SAGA complex and NPC components in recruitment of the *GAL* locus to the nuclear periphery. However, we extended this finding and demonstrate that these complexes play a more global role in chromosome organization. Furthermore, we provide evidence that both complexes are involved

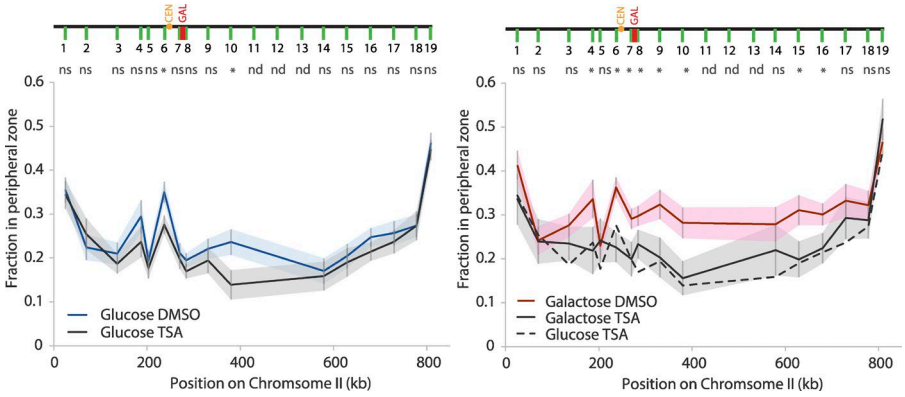

Figure 7. **HDAC activity is required for chromosome reorganization.** Chr II library yeast strains were grown overnight in medium with glucose or galactose as a carbon source in the presence of 50 µM TSA or solvent only (1% DMSO). Fraction at the nuclear periphery is plotted relative to the position on the chromosome, with shaded areas corresponding to 95% confidence intervals. *, $P < 0.01$; ns, not significant ($P > 0.01$); nd, not determined for two-proportions *z* test. Data are pooled from three or more independent experiments (>50 cells each).

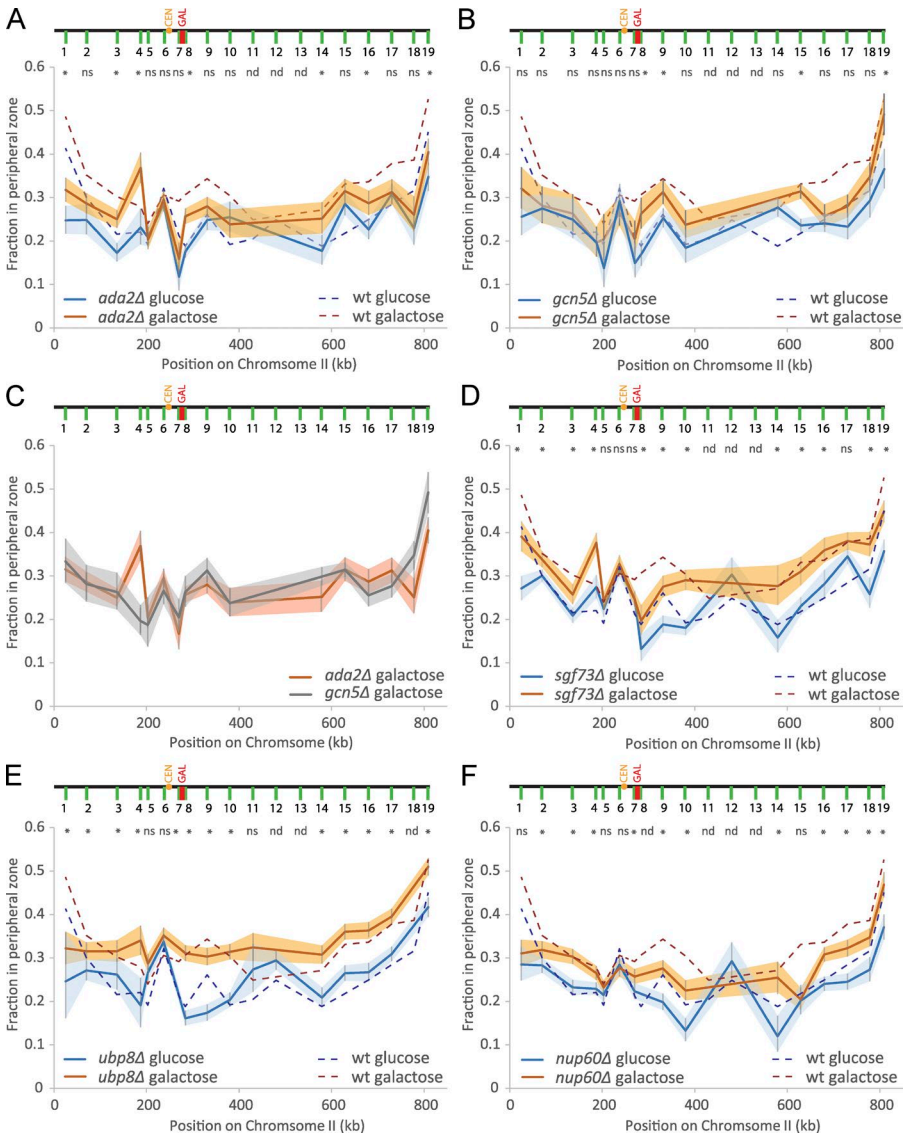

Figure 8. **Fraction of peripheral loci in mutants grown in glucose (blue) or galactose (orange).** (A) *ada2Δ*. (B) *gcn5Δ*. (C) Overlay of *ada2Δ* and *gcn5Δ* in galactose. (D) *sgf73Δ*. (E) *ubp8Δ*. (F) *nup60Δ*. Shaded areas indicate 95% confidence interval. *, P < 0.01; ns, not significant (P > 0.01); nd, not determined for two-proportions *z* test. Dashed lines indicate levels in wild type (as in Fig. 2 A): blue, glucose; red, galactose. Data are pooled from three or more independent experiments (>50 cells each).

in telomere tethering to the periphery. We find that the HAT activity of SAGA, but not its deubiquitination activity, is required for nuclear envelope association of chr II. Finally, our genome-wide screen uncovered a role of HDACs in chromatin organization, and our results revealed the existence of a common mechanism for peripheralization along the entire chr II requiring both HAT and HDAC activity.

Discussion

High-throughput methods for chromatin analysis

To thoroughly and systematically analyze the function and organization of chromatin, high-throughput methods are required. Here, we used chromatin tagging, imaging, and automated analysis techniques to develop a platform for high-throughput strain generation and robust data analysis. This enabled us to perform a systematic analysis of the spatial organization of a yeast chromosome within living cells. Our analysis uncovered a global chromatin reorganization process that is linked to changes in cellular physiology and has a major impact on the 3D organization of the nucleus. The process is regulated by the opposing activities of HAT and HDAC complexes. Our results provide new insights into the mechanism of *GAL* locus localization and furthermore suggest that peripheral anchoring may be a more prevalent phenomenon than previously thought.

For our analyses, we made use of the yeast deletion collection to integrate an identical LacO-cassette in multiple loci within the genome, allowing us to systematically label different positions in a single-step procedure. Although this enabled the rapid generation of many strains in parallel, this approach has the drawback that every strain harbors the deletion of a distinct ORF. Here, we used strains that had no obvious growth phenotype and that were not annotated with strong phenotypes on www.yeastgenome.org. Furthermore, by examining many strains in parallel, we could disregard effects that were seen in individual strains, but not in neighboring control strains. Nevertheless, the mutant background remains a caveat and might be avoided in future applications, e.g., by using different types of collections with identical inserts in different genome positions or by the use of heterozygous diploid strains.

Our analysis was greatly aided by automated imaging and the analysis pipeline that we present here. These tools were

essential for us to perform our large-scale analysis experiments, but they should also be of more general use for the community to analyze gene position and movement in an unbiased and highly automated manner.

Physiological states globally affect chromatin architecture

In our study, we uncovered wide-ranging alterations in chromatin organization on changes in carbon source. We find that the recruitment of the *GAL* locus to the nuclear periphery is not a singular event. Based on our results with computational modeling, an artificial tether, and the *GAL* locus deletion strains, we propose that additional anchoring sites must exist on the same chromosome even in close neighborhood to the *GAL* locus, and most likely on other chromosomes. In agreement with this, previous chromatin precipitation experiments identified genes that show increased interactions with NPC proteins in galactose compared with glucose (Casolari et al., 2004). However, the absolute number of genes that showed this behavior was small, supporting the idea that only a few distinct stable tethering sites might exist.

What defines those tethering sites? What is their function? In glucose, >4,000 genes are actively expressed, and if tethering sites are linked to transcriptional activation, this would argue that only very few selected loci associate with NPCs when active. This notion could be supported by the observation that specific DNA zip codes can target genes to the nuclear envelope (Ahmed et al., 2010). Alternatively, the fact that no specific tethering sites are observed in glucose could be associated with the high overall transcriptional output of these cells. In these conditions, transcribing loci may compete for the association with the nuclear periphery. In addition, these events may be widely distributed over the entire genome and differ from cell to cell so that no net enrichment can be detected in a population. Only on reduction of the overall transcriptional output, specific genes that are highly transcribed might stand out and can be detected in the population. This idea would be consistent with chromatin immunoprecipitation experiments with NPC components in which the transcriptional activity of a gene correlated with its association with nucleoporins (Casolari et al., 2004). Alternatively, attachment sites at the nuclear envelope might not be available in fast-growing fermenting cells and might only become activated on a shift to respiration, e.g., by posttranslational modification of nucleoporins. Potentially interesting in this context is the requirement of HAT and HDAC activities for chromatin peripheralization because the global acetylation state can be a signal for the metabolic state of the cell (Cai et al., 2011), potentially providing a regulatory mechanism for chromatin association with the nuclear periphery.

Alternatively, association with the nuclear periphery might not be primarily related to gene activation but to gene repression. *S. cerevisiae* divides optimally on glucose using fermentation to generate all ATP for cellular growth and function. In contrast, growth on galactose or raffinose is considerably slower, and cells use both fermentation and respiration (Fendt and Sauer, 2010). Apart from the large number of gene expression changes occurring on shift from glucose to another carbon source (Gasch and Werner-Washburne, 2002), the slower growth rate would also be expected to require overall lower metabolic rates and therefore lower levels of gene activity. In this context, peripheralization could contribute to repression because the periphery does not only harbor the repressive environment for telomere silencing, but the association of the *GAL* locus with the nuclear periphery has also been shown to dampen expression (Green et al., 2012).

Importantly, not all of the interaction points with the nuclear periphery may be of the same nature as indicated by the local effects of, e.g., the *sgf73Δ* and *nup60Δ* mutants. Therefore, a combination of activating and repressing mechanisms for chromatin association with the nuclear periphery is possible. Additional experiments will be needed to differentiate between these models and to better understand the functional role of the gene attachment at the nuclear periphery and the NPC.

Role of SAGA in chromatin organization

Our analysis uncovered a global role for the histone acetylation complex SAGA in chromatin organization in galactose-growing cells. Deletion of SAGA components significantly affects the expression of up to 10% of the yeast genome, but SAGA is involved in the regulation of many more genes (Lee et al., 2000). The complex combines an acetylation module and a deubiquitinaton module and has been implicated in various transcription-associated processes, including activation, elongation, and spliceosome assembly (Koutelou et al., 2010). In addition, Sgf73 links SAGA and the mRNA export complex TREX-2 (Köhler et al., 2008). The fact that we observe a reduced peripheral association of different chromosome regions with the nuclear periphery in *gcn5Δ* and *ada2Δ* mutants suggests that peripheralization of chr II in galactose depends on the HAT function of the SAGA complex, which is involved both in transcriptional activation and elongation (Balasubramanian et al., 2002; Govind et al., 2007). In contrast, the deubiquitinase function is not required because deletion of *SGF73* or the deubiquitinase *UBP8* did not have an effect on global peripheralization in galactose. Nevertheless, deletion of *SGF73* did affect peripheral localization of the *GAL* locus, supporting previous results that implicate a physical interaction between SAGA and mRNA export in *GAL* localization at the nuclear periphery (Köhler et al., 2008). In addition, *gcn5Δ* cells still showed an increased localization at the nuclear periphery in galactose compared with glucose, again pointing to the presence of tethers with different mechanisms.

Anchoring of telomeres

The interaction of telomeres with the nuclear periphery has been the subject of several studies and involves multiple pathways, including the interaction of Sir proteins with the inner nuclear membrane protein Esc1 (Andrulis et al., 2002; Taddei et al., 2004) and the interaction of yKu70 with components of the nuclear basket of the NPC Mlp1, Mlp2, and Nup60 (Galy et al., 2000; Feuerbach et al., 2002). However, the involvement of Mlp1/2 in telomere anchoring has been debated (Hediger et al., 2002a,b). We find here that the deletion of Nup60 indeed affects localization of at least a subset of telomeres to the nuclear periphery because the left telomere of chr II lost its preferential peripheral localization in *nup60Δ* cells. However, no significant effect on the right telomere was observed. Such telomere-specific effects could explain the discrepancies described in previous studies. In addition, we observed strong effects on anchoring of the left telomere in the SAGA complex mutants. A role of SAGA in telomere anchoring is in line with the observation that SAGA is required for the silencing of telomeres (Jacobson and Pillus, 2009).

HDAC activity in gene tethering at the nuclear periphery

In our screen, we uncovered a novel role of HDACs in tethering the *GAL* locus at the nuclear periphery and further showed that HDAC activity is globally involved in the rearrangement of chromatin that occurs in cells that are grown in the absence of glucose. Interestingly, HDAC inhibition by TSA also had a specific effect on centromere localization in glucose. Globally, both acetylation and deacetylation are required for the peripheralization process. We can only speculate on the targets that are modified by these activities. Although histones are obvious candidates, the modification of other proteins could also be involved in establishing a tether between chromatin and the nuclear envelope. In higher eukaryotes, HATs and HDACs can bind directly to nuclear pore or nuclear envelope proteins (Somech et al., 2005; Kehat et al., 2011; Demmerle et al., 2012). Furthermore, treatment of human cells with TSA leads to a characteristic increase of acetylation in a zone underlying the nuclear envelope (Taddei et al., 2001) and changes in the interaction pattern of genomic sequences with the nucleoporin Nup93 (Brown et al., 2008). Although specific localization of HATs and HDACs has not been reported in yeast, our findings clearly indicate that these enzymatic activities have important functions in linking chromatin to the nuclear envelope. In this context, it is intriguing that NPCs have also been shown to act as boundary elements (Ishii et al., 2002), which are thought to be associated with both HAT and HDAC activities to prevent the spreading of repressive and activating marks along the chromatin.

Materials and methods

Plasmid construction

Plasmids were constructed using standard molecular biology techniques. The plasmid for replacing the KanMX cassette in deletion strains (pKW2832) was constructed by ligating PCR products containing the 3′ and 5′ MX cassette modules with a BglII site in between into pKW1689 (placOp-YBR022W-LEU2; Green et al., 2012) replacing the YBR022W homology region (Fig. 1 B). The cassette was amplified from pKW2668 using primer UC4896 and UC4897 and cloned into pKW1689 using XhoI and SacI. pKW2668 was constructed by cloning the PCR product of UC4236/UC4237 encompassing the 3′ MX cassette of pFA6a-KanMX (Bähler et al., 1998) into pKW2572 (pRS306-HphMX; gift from J. Thorner, University of California, Berkeley, Berkeley, CA), which contains the hygromycin resistance marker with a 5′ MX cassette. pKW2623 was constructed by cloning of GFP-LacI amplified from pKW760 (Green et al., 2012) using primers UC4080/UC4081 into pKW2572 using NsiI and ClaI. pKW2627 was generated by stitching the PCR product of primers UC3286/UC3915 on pKW1456 (pNatMX-switch(p4339); Tong et al., 2001) and the PCR product of UC4096 and UC4115 on pKW2579 (RPL25NLS-CFP under *CYC1* promoter) using UC3286/UC4115 and ligating into pGem-T (Roche). pKW2579 was generated by ligating a PCR product of UC3943/UC3944 on genomic DNA into pKW2574 using NotI and EcoRI to replace the promoter with the low expressing *CYC1* promoter. pKW2574 was generated by ligating RPL25NLS-CFP with the *TPI1* promoter cut from pKW2561 with NotI and SalI into pRS404 using the same enzymes. pKW2561 was generated by three-fragment ligation of PCR product of UC3904 and UC3905 on pKW809 (pRPL25N-LS-GFP; Timney et al., 2006) cut NotI–BglII (RPL25NLS with the *TPI1* promoter), PCR product of oligos UC3906 and UC3907 on pKW2103 (pKT210) cut with BglII–HindIII (yeast optimized enhanced CFP), and pKW349 (pRS315) cut NotI–HindIII.

The LacO integration plasmids for different genomic loci were cloned by integration of a PCR product on genomic DNA into pKW1689 cut with XhoI and SacI: pKW2649 with primers UC4244/UC4245, pKW2650 with primers UC4246/UC4247, pKW2653 with primers UC4234/UC4235, pKW2654 with UC4265/UC4266, pKW2664 with UC4372/UC4373, and pKW2665 with UC4376/UC4377.

Plasmids for integration of TetO repeats at *POA1* (pKW2837) or *SEC66* (pKW3147) were derived from pKW2526 (p306tetO112; Michaelis et al., 1997) by insertion of a PCR product of UC4155/UC4766 (*POA1*) or UC6032/UC6033 (*SEC66*) into the SacI site.

Plasmids are listed in Table S1. Primers are listed in Table S2.

Yeast strain construction

Strains were constructed using standard yeast genetic techniques either by transformation of a linearized plasmid or of a PCR amplification product with homology to the target site (Baudin et al., 1993). The fluorescent marker strain containing Ndc1-tdTomato, RPL25NLS-CFP, and GFP-LacI was constructed by sequential integration of all markers at the *NDC1* locus to reduce the usage of selection markers. First, in the synthetic genetic array (SGA) query strain Y7092, *NDC1* was tagged with tdTomato at the endogenous locus by transformation with a PCR product generated with primers UC3741 and UC3742 on plasmid pKW1812 (tdTomato ligated into pKT127 using AscI and PacI; gift from J. Thorner) yielding KWY2782. Next, pKW2623 cut NsiI–HindIII and containing LacI-GFP, and a hygromycin resistance cassette was integrated to replace the KanMX cassette from the tdTomato tagging yielding KWY2816. Finally, the hygromycin resistance cassette was replaced by integration of pKW2627 cut with SacII and NotI containing RPL25NLS-CFP and a resistance cassette for nourseothricin (ClonNat). This yielded strain KWY2825, which was the base strain containing all fluorescent markers.

KWY2825 was transformed with plasmid pKW1689 (Green et al., 2012) for integration of 256 LacO repeats at POA1 (5 kb telomeric of the *GAL1* gene) to yield KWY2823. This strain was used to cross into the deletion collection for screening (see Genome-wide screen).

Additional insertions of LacO repeats on other chromosomes were performed by transformation of linearized plasmids into KWY2825: at *INO1* with pKW1698 (p6INOlac128; Brickner and Walter, 2004) linearized BglII yielding KWY2824; at *RPL9A* with pKW2649 linearized with AgeI yielding KWY2872; at *HXK1* with pKW2650 linearized with NsiI yielding KWY2873; at *RPL25* with pKW2653 linearized with PacI yielding KWY2875; at *ADH4* with pKW2654 linearized with PacI yielding KWY2884; at *PES4* with pKW2664 linearized with BglII yielding KWY2960; and at *FIG2* with pKW2665 linearized with SpeI yielding KWY2961.

Mutants in KWY2823 carrying the 256 LacO repeats were generated by transformation of PCR product on pKW1008 to replace the ORF with a KanMX cassette. *Δrpd3*: UC4268/UC4269 → KWY3611; *Δhda1*: UC4264/UC4289 → KWY3610; *Δrco1*: UC5411/UC5412 → KWY3612; and *sds3Δ*: UC5409/UC5410 → KWY3613.

Strains marked on chr II were constructed by mating the deletion strains (*ybl101c*, *ybl083c*, *ybl044w*, *ybl017c*, *ybl012c*, *ybl001c*, *ybr016w*, *ybr022w*, *ybr046c*, *ybr071w*, *ybr093c*, *ybr120c*, *ybr144c*, *ybr172c*, *ybr203w*, *ybr230c*, *ybr258c*, *ybr288c*, and *ybr300c*) from the haploid MATa deletion collection to the fluorescent marker strain KWY2825 and then transforming with the LacO plasmid pKW2832. Clones that had acquired *LEU2* autotrophy and lost geneticin resistance were checked for visible LacO–LacI signal under the microscope and then sporulated and selected for haploids containing all markers via SGA selection procedures following the protocol in Tong and Boone (2007). In some cases, tetrad dissection was performed to select haploid clones. Correct integration of the LacO-plasmid was checked

by PCR. This yielded strains KWY3354-KWY3370, KWY3403, KWY3947, and KWY4019. No clones for *ybr144c* were obtained. Mutants of chr II strains were constructed by mating and sporulation with the mutant strains generated by transformation of a PCR product into the KWY2825 background replacing the ORF with a KanMX cassette (*gnc5*: oligos UC5348/UC5349 on pFA6a-KanMX6 → KWY4140, *ada2*: UC1977/UC2165 on pFA6a-KanMX6 → KWY3965, *sgf73*: UC5899/UC5898 on genomic DNA from deletion collection strain → KWY4092, *ubp8*: UC4404/UC4405 on pFA6a-KanMX6 → KWY4137, and *nup60*: UC3170/UC3171 on genomic DNA from deletion collection strain → KWY4135). Deletions were checked by PCR.

For deletion of the *GAL7-GAL10-GAL1* locus, a PCR product of UC5487/UC5488 on pFA6a-KanMX6 was transformed into strains of the chr II library KWY3356, KWY3358, KWY3361, KWY3362, KWY3363, KWY3364, and KWY3366 and into the base marker strain KWY2825 to replace the entire *GAL* locus encompassing bp 274203–281017 with a KanMX cassette yielding strains KWY4014, KWY44001, KWY4055, KWY4054, KWY4098, KWY3821, KWY4015, and KWY3365. Each mutant strain was mated to KWY2825 and each corresponding wild-type strain to KWY3365 to yield the diploids used in the experiment.

TetO repeats were integrated into strains of the chr II library by transformation with pKW2837 linearized by BlpI (integration at *POA1*) or pKW3147 linearized with EcoRI (integration at *SEC66*). For the artificial tether strains, strains with TetO repeats integrated at *POA1* were mated with KWY5251 in which *MLP1* was tagged with TetR by integration of a PCR product with primers CH698 and CH645 on pKW3500 (Kiermaier et al., 2009), sporulated, and tetrad dissected. To prevent any potential toxic effect of chromosome tethering to the nuclear periphery, all steps where performed on media containing 10 µg/ml doxycycline, and cells were maintained in this media until 16 h before the experiment.

Genotypes of all strains used are listed in Table S3.

Yeast culture conditions

For all microscopy experiments, cells were pregrown in synthetic complete (SC) medium with 2% raffinose for 3 d at RT, inoculated into SC with the appropriate carbon source (2% glucose, galactose, or raffinose), and grown for 16–19 h at RT to ODs of 0.2–0.8. For experiments with many samples, cells were grown on a shaker in 96 well plates with one 4-mm glass bead per well. Imaging was performed in glass-bottom 384-well plates (Matrical) coated with concanavalin A to immobilize the cells.

Microscopy

Microscopy for localization of genomic loci relative to the nuclear periphery was performed on an inverted epifluoresence Ti microscope (Nikon) equipped with an Intensilight mercury light source and a Clara charge coupled device (CCD) camera (Andor) using 60× or 100× total internal reflection fluorescence objectives, NA 1.49 (Nikon), and Metamorph software (Molecular Devices). Experiments for Figs. 3 B and 5 B were performed on an inverted epifluoresence Ti microscope equipped with a Spectra X LED light source (Lumencore) and a Flash 4.0 scMOS camera (Hamamatsu) using a 100× Plan-Apo VC objective NA 1.4 (Nikon) and NIS Elements software (Nikon).

3D microscopy for compaction analysis (Fig. 4 B) was performed on a spinning disk confocal microscope. The Yokogawa spinning disk head was mounted on a Nikon Ti-inverted microscope body. Fluorescent molecules were excited by solid-state diode lasers of 488 and 561 nm. Images were acquired with a Clara CCD camera using a 100× Plan-Apo objective NA 1.4. The microscope was controlled by Metamorph. All microscopy was performed at RT.

Automated image analysis of gene localization

Automated image analysis of gene localization relative to the nuclear envelope was performed using custom-written MATLAB (MathWorks) code. In brief, cells were detected by thresholding NLS-CFP, Ndc1-td-Tomato, and GFP-LacI channels, and only cells with all three components were analyzed. Gene dots were localized by a 2D Gaussian fit. The nuclear periphery was defined by first fitting the Ndc1-tdTomato signal with an ellipse and then refining the nuclear envelope trace. Importantly, the refined computation was performed in polar coordinates around the preliminary ellipse center. This avoided a bias toward smaller nuclear size. In particular, linear interpolation of the edge in dim segments and the final smoothing of the boundary line would both have created a systematic underestimation of the true nuclear size, but in polar coordinates this error source is naturally absent.

Points on the nuclear envelope were first defined at the global signal maximum along each ray from the ellipse center. In dim segments, where the maximum was below a threshold, positions were interpolated between neighbors with a strong signal. In a second step, all local signal maxima along the initial nuclear envelope trace were fixed as reliable anchor points. Between these anchor points, a second curve was formed by cubic spline interpolation, with tangent directions coming from the tangents at the first curve. A combined curve was defined in each radial direction by the candidate with greater distance from the center. The spline interpolation in the second step was designed to avoid another source of systematic underestimation of nuclear size: where the signal is not continuous along the nuclear envelope, but consists of interrupted segments, the blurred segments might fuse in a way that the radial signal maxima lie considerably inside the actual shape. Finally, the combined curve was smoothed by a moving average filter.

On the final nuclear outline, the point closest to the gene dot was determined, and the distance of this point to the gene dot was normalized by its distance to the center of the initially fit ellipse to correct for differences in nuclear size and cross-sectional plane. Negative distances occasionally occurred because the center of the gene dot was localized just outside of the nuclear envelope trace. Only experiments with at least 50 cells but typically 150–300 cells analyzed were taken into consideration. Each experiment was independently repeated at least three times. Generalized linear models with a binomial distribution (dot localized within or outside of a peripheral zone of 0.1835 times the radius) and logit link function were used to analyze the contribution of day-to-day variability and nuclear size on the data. Both parameters showed significant contributions to the localization only in very few strains and were therefore not further considered (compare Fig. S1 D for analysis of the restricted nuclear size bin). P values given in figures are derived from a two-proportions z test. In the adaptation for z-stack analysis (Fig. S1 B), the position of gene loci was initially identified on z projections, and each nucleus was then analyzed on the plane with the highest gene locus signal.

Gene localization for compaction analysis (Fig. 4 B) was performed using Imaris (Bitplane). Images were first smoothed by convolution with a Gaussian filter. Gene dots were then detected using the spot detection mode of Imaris, and the thresholds were manually adjusted for each individual set of images. Dot positions were then exported and further processed in MATLAB to yield the distance between the dots in the two channels for each cell. Any additional calculations and statistical analyses were performed in MATLAB or Excel (Microsoft).

Genome-wide screen

Generation of the screening library was achieved using SGA techniques (Tong et al., 2001; Young and Loewen, 2013). Strain KWY2823 was mated to the haploid deletion collection of nonessential genes using a RoToR HDA robot (Singer Instruments) at a density of 1,536 spots per

plate. After selection of diploids, strains were sporulated, and haploid progeny were generated containing the LacO array, fluorescent marker proteins, and corresponding genomic deletion by selection on SD-His/Arg/Lys/Leu media containing 200 µg/ml G418 sulfate and 100 µg/ml nourseothricin ("clonNAT"; Werner Biotech), 50 µg/ml canavanine, and 50 µg/ml thialysine.

For microscopy, this reporter library was grown in 96 plates as described in Yeast Culture Conditions in galactose medium. Cells were transferred to 384-well glass bottom plates coated with concanavalin A and fixed with 4% formaldehyde solution for 20 min, washed three times with PBS, and sealed. Imaging was performed in PBS on the same day of fixation using a Nikon 60× oil-immersion total internal reflection fluorescence objective, NA 1.49, on a TiE epifluorescent microscope equipped with an Andor Clara CCD camera. Images were analyzed automatically as described in Automated image analysis of gene localization. All wells with >50 cells counted were included in the analysis. This yielded results for 4,219 and 4,480 unique gene deletions in two biological replicates of the screen, of which 4,122 were valid in both replicates (Table S4). Z scores for a fraction of cells with *GAL* localization at the nuclear periphery (closer than 2 px corresponding to 215 nm) were calculated per 96-well plate. All genes that had a Z score less than −2 in each of the two biological repeats were included in the hit list shown in Fig. 6 A (114 genes).

Computational modeling

The haploid yeast genome models were generated as described previously (Tjong et al., 2012). The 16 chromosomes are represented as chains of connecting beads with a diameter of 30 nm. Each bead accommodates ∼3.2 kb of genome sequence. The ∼12-Mb yeast genome is represented by a total of 3,779 beads. The nuclear radius is set to 1 µm. The SPB and nucleolus are located at opposite ends of the nucleus, whereas a central axis connects the centers of the SPB, nucleus, and nucleolus. We optimize the location of chromosomes, whereas locations of the SPB and nucleolus remain fixed. Centromeres are restricted to be near SPB, whereas telomeres are within 50 nm from the nuclear envelope.

The scoring function is defined as a sum of spatial restraints, which quantifies the degree of consistency between the structure and the imposed restraints derived from experimental information (Tjong et al., 2012). The optimization is performed as described in Tjong et al. (2012), by using a combination of simulated annealing dynamics and the conjugate gradient methods implemented in the Integrated Modeling Platform (Russel et al., 2012). An individual optimization starts with an entirely random bead configuration, followed by an initial optimization of the structure and subsequent simulated annealing protocols to entirely equilibrate the genome configuration. Finally, conjugate gradient optimization ensures that all constraints are satisfied, leading to a structure with a score of zero. Many independent optimizations each starting from random bead configurations are performed to generate a population of 1,000 genome structures with a total score of zero and hence are consistent with all input data.

Nuclear envelope tethering of specific loci (*GAL*-pro and *ybr203w*). In addition to the wild-type (control) genome models, we also generated models in which loci were specifically tethered to the nuclear envelope. In addition to the restraints in the wild-type model, these models also included locus nuclear envelope (NE) tethering restraints. Similar to telomeres, the bead representing the tethered locus is positioned in the vicinity of the nuclear envelope by applying a lower bound harmonic function:

$$U_{NE\text{-}loc} = \begin{cases} \frac{1}{2}(\|r_{loc}\| - 950\,nm)^2, for\ \|r_{loc}\| < 950\,nm \\ 0, otherwise \end{cases},$$

where $\|r_{loc}\|$ is the distance of the locus from the center of the nucleus.

Chromosome models with increased compaction. To simulate a higher chromatin compaction, a chromatin bead was represented with a slightly larger diameter (40 nm), which accommodated 7,600 bp per bead. This model resulted in chromatin chains with a total of 1,595 beads for all 16 chromosomes. The chromosomes are constrained in a manner identical to the wild-type population.

Cell cycle analysis

Cell cycle analysis was performed by flow cytometry according to Haase (2004). In brief, cells were fixed with 70% ethanol, treated with RNase and trypsin, and stained with SYTOX Green (Molecular Probes) and analyzed on a BD FACSCalibur flow cytometer.

Gene expression analysis

Cells were harvested by centrifugation and snap frozen in liquid nitrogen. RNA was extracted using the RNeasy kit (QIAGEN) via mechanical disruption. 300 ng of total extracted RNA was used for reverse transcription. The RNA was first treated with DNase I using the DNA-free kit (Ambion) according to the protocol of the manufacturer. Reverse transcription was performed according to the protocol of the manufacturer using Superscript II reverse transcriptase (Invitrogen) with random hexamer primers. Quantitative real-time PCR was performed on a StepOnePlus Instrument (Invitrogen) using Absolute Blue QPCR Mix with SYBR Green and ROX (Thermo Fisher Scientific). All experiments were performed in three technical replicates and three biological replicates. Data were analyzed by the comparative cycle threshold method using *ACT1* as endogenous control.

Online supplemental material

Plasmids, primers, and yeast strains used are provided in Tables S1, S2, and S3, respectively. Table S4 presents a summary of the results from the genome-wide imaging screen of *GAL* locus position relative to the nuclear envelope. Fig. S1 presents the comparison of manual and automated image analysis and an analysis illustrating that nuclear size does not strongly contribute to the observed shift toward the nuclear periphery. Fig. S2 presents histograms of distance distributions for all loci analyzed on chr II and for additional loci on other chromosomes. Fig. S3 presents modeling results for tethered chr II without (A) and with (B) additional compaction and linear distances along the chromosomes expected from these models (C). Fig. S4 shows results from gene expression and cell cycle analysis for HDAC mutants and TSA treatment. Online supplemental material is available at http://www.jcb.org/cgi/content/full/jcb.201507069/DC1.

Acknowledgments

We thank Colleen McGourty and Megan Hochstrasser for help with strain construction, Alan Lowe for help with MATLAB coding, and members of the Weis group, Monika Mayr, and Yves Barral for critical reading of the manuscript.

This work was supported by a European Molecular Biology Organization long-term fellowship (ALTF 182-2010 to E. Dultz), the National Institutes of Health/National Institute of General Medical Sciences (R01GM058065 to K. Weis), and the Arnold and Mabel Beckman foundation/National Science Foundation (1150287 to F. Alber).

The authors declare no competing financial interests.

Submitted: 16 July 2015
Accepted: 5 January 2016

References

Abruzzi, K.C., D.A. Belostotsky, J.A. Chekanova, K. Dower, and M. Rosbash. 2006. 3′-end formation signals modulate the association of genes with the nuclear periphery as well as mRNP dot formation. *EMBO J.* 25:4253–4262. http://dx.doi.org/10.1038/sj.emboj.7601305

Ahmed, S., D.G. Brickner, W.H. Light, I. Cajigas, M. McDonough, A.B. Froyshteter, T. Volpe, and J.H. Brickner. 2010. DNA zip codes control an ancient mechanism for gene targeting to the nuclear periphery. *Nat. Cell Biol.* 12:111–118. http://dx.doi.org/10.1038/ncb2011

Albert, B., J. Mathon, A. Shukla, H. Saad, C. Normand, I. Léger-Silvestre, D. Villa, A. Kamgoue, J. Mozziconacci, H. Wong, et al. 2013. Systematic characterization of the conformation and dynamics of budding yeast chromosome XII. *J. Cell Biol.* 202:201–210. http://dx.doi.org/10.1083/jcb.201208186

Andrulis, E.D., D.C. Zappulla, A. Ansari, S. Perrod, C.V. Laiosa, M.R. Gartenberg, and R. Sternglanz. 2002. Esc1, a nuclear periphery protein required for Sir4-based plasmid anchoring and partitioning. *Mol. Cell. Biol.* 22:8292–8301. http://dx.doi.org/10.1128/MCB.22.23.8292-8301.2002

Bähler, J., J.Q. Wu, M.S. Longtine, N.G. Shah, A. McKenzie III, A.B. Steever, A. Wach, P. Philippsen, and J.R. Pringle. 1998. Heterologous modules for efficient and versatile PCR-based gene targeting in *Schizosaccharomyces pombe*. *Yeast.* 14:943–951. http://dx.doi.org/10.1002/(SICI)1097-0061(199807)14:10<943::AID-YEA292>3.0.CO;2-Y

Balasubramanian, R., M.G. Pray-Grant, W. Selleck, P.A. Grant, and S. Tan. 2002. Role of the Ada2 and Ada3 transcriptional coactivators in histone acetylation. *J. Biol. Chem.* 277:7989–7995. http://dx.doi.org/10.1074/jbc.M110849200

Bash, R., and D. Lohr. 2001. Yeast chromatin structure and regulation of GAL gene expression. *Prog. Nucleic Acid Res. Mol. Biol.* 65:197–259. http://dx.doi.org/10.1016/S0079-6603(00)65006-7

Baudin, A., O. Ozier-Kalogeropoulos, A. Denouel, F. Lacroute, and C. Cullin. 1993. A simple and efficient method for direct gene deletion in *Saccharomyces cerevisiae*. *Nucleic Acids Res.* 21:3329–3330. http://dx.doi.org/10.1093/nar/21.14.3329

Berger, A.B., G.G. Cabal, E. Fabre, T. Duong, H. Buc, U. Nehrbass, J.C. Olivo-Marin, O. Gadal, and C. Zimmer. 2008. High-resolution statistical mapping reveals gene territories in live yeast. *Nat. Methods.* 5:1031–1037. http://dx.doi.org/10.1038/nmeth.1266

Bickmore, W.A., and B. van Steensel. 2013. Genome architecture: domain organization of interphase chromosomes. *Cell.* 152:1270–1284. http://dx.doi.org/10.1016/j.cell.2013.02.001

Brickner, D.G., and J.H. Brickner. 2010. Cdk phosphorylation of a nucleoporin controls localization of active genes through the cell cycle. *Mol. Biol. Cell.* 21:3421–3432. http://dx.doi.org/10.1091/mbc.E10-01-0065

Brickner, J.H., and P. Walter. 2004. Gene recruitment of the activated INO1 locus to the nuclear membrane. *PLoS Biol.* 2:e342. http://dx.doi.org/10.1371/journal.pbio.0020342

Brown, C.R., C.J. Kennedy, V.A. Delmar, D.J. Forbes, and P.A. Silver. 2008. Global histone acetylation induces functional genomic reorganization at mammalian nuclear pore complexes. *Genes Dev.* 22:627–639. http://dx.doi.org/10.1101/gad.1632708

Cabal, G.G., A. Genovesio, S. Rodriguez-Navarro, C. Zimmer, O. Gadal, A. Lesne, H. Buc, F. Feuerbach-Fournier, J.C. Olivo-Marin, E.C. Hurt, and U. Nehrbass. 2006. SAGA interacting factors confine sub-diffusion of transcribed genes to the nuclear envelope. *Nature.* 441:770–773. http://dx.doi.org/10.1038/nature04752

Cai, L., B.M. Sutter, B. Li, and B.P. Tu. 2011. Acetyl-CoA induces cell growth and proliferation by promoting the acetylation of histones at growth genes. *Mol. Cell.* 42:426–437. http://dx.doi.org/10.1016/j.molcel.2011.05.004

Casolari, J.M., C.R. Brown, S. Komili, J. West, H. Hieronymus, and P.A. Silver. 2004. Genome-wide localization of the nuclear transport machinery couples transcriptional status and nuclear organization. *Cell.* 117:427–439. http://dx.doi.org/10.1016/S0092-8674(04)00448-9

Demmerle, J., A.J. Koch, and J.M. Holaska. 2012. The nuclear envelope protein emerin binds directly to histone deacetylase 3 (HDAC3) and activates HDAC3 activity. *J. Biol. Chem.* 287:22080–22088. http://dx.doi.org/10.1074/jbc.M111.325308

Denoth-Lippuner, A., M.K. Krzyzanowski, C. Stober, and Y. Barral. 2014. Role of SAGA in the asymmetric segregation of DNA circles during yeast ageing. *eLife.* 3:3. http://dx.doi.org/10.7554/eLife.03790

Dieppois, G., N. Iglesias, and F. Stutz. 2006. Cotranscriptional recruitment to the mRNA export receptor Mex67p contributes to nuclear pore anchoring of activated genes. *Mol. Cell. Biol.* 26:7858–7870. http://dx.doi.org/10.1128/MCB.00870-06

Fendt, S.M., and U. Sauer. 2010. Transcriptional regulation of respiration in yeast metabolizing differently repressive carbon substrates. *BMC Syst. Biol.* 4:12. http://dx.doi.org/10.1186/1752-0509-4-12

Feuerbach, F., V. Galy, E. Trelles-Sticken, M. Fromont-Racine, A. Jacquier, E. Gilson, J.C. Olivo-Marin, H. Scherthan, and U. Nehrbass. 2002. Nuclear architecture and spatial positioning help establish transcriptional states of telomeres in yeast. *Nat. Cell Biol.* 4:214–221. http://dx.doi.org/10.1038/ncb756

Galy, V., J.C. Olivo-Marin, H. Scherthan, V. Doye, N. Rascalou, and U. Nehrbass. 2000. Nuclear pore complexes in the organization of silent telomeric chromatin. *Nature.* 403:108–112. http://dx.doi.org/10.1038/47528

Gasch, A.P., and M. Werner-Washburne. 2002. The genomics of yeast responses to environmental stress and starvation. *Funct. Integr. Genomics.* 2:181–192. http://dx.doi.org/10.1007/s10142-002-0058-2

Govind, C.K., F. Zhang, H. Qiu, K. Hofmeyer, and A.G. Hinnebusch. 2007. Gcn5 promotes acetylation, eviction, and methylation of nucleosomes in transcribed coding regions. *Mol. Cell.* 25:31–42. http://dx.doi.org/10.1016/j.molcel.2006.11.020

Green, E.M., Y. Jiang, R. Joyner, and K. Weis. 2012. A negative feedback loop at the nuclear periphery regulates GAL gene expression. *Mol. Biol. Cell.* 23:1367–1375. http://dx.doi.org/10.1091/mbc.E11-06-0547

Haase, S.B. 2004. Cell cycle analysis of budding yeast using SYTOX Green. Curr. Protoc. Cytom. Chapter 7:Unit 7 23.

Hediger, F., K. Dubrana, and S.M. Gasser. 2002a. Myosin-like proteins 1 and 2 are not required for silencing or telomere anchoring, but act in the Tel1 pathway of telomere length control. *J. Struct. Biol.* 140:79–91. http://dx.doi.org/10.1016/S1047-8477(02)00533-6

Hediger, F., F.R. Neumann, G. Van Houwe, K. Dubrana, and S.M. Gasser. 2002b. Live imaging of telomeres: yKu and Sir proteins define redundant telomere-anchoring pathways in yeast. *Curr. Biol.* 12:2076–2089. http://dx.doi.org/10.1016/S0960-9822(02)01338-6

Ishii, K., G. Arib, C. Lin, G. Van Houwe, and U.K. Laemmli. 2002. Chromatin boundaries in budding yeast: the nuclear pore connection. *Cell.* 109:551–562. http://dx.doi.org/10.1016/S0092-8674(02)00756-0

Jacobson, S., and L. Pillus. 2009. The SAGA subunit Ada2 functions in transcriptional silencing. *Mol. Cell. Biol.* 29:6033–6045. http://dx.doi.org/10.1128/MCB.00542-09

Jani, D., E. Valkov, and M. Stewart. 2014. Structural basis for binding the TREX2 complex to nuclear pores, GAL1 localisation and mRNA export. *Nucleic Acids Res.* 42:6686–6697. http://dx.doi.org/10.1093/nar/gku252

Jin, Q.W., J. Fuchs, and J. Loidl. 2000. Centromere clustering is a major determinant of yeast interphase nuclear organization. *J. Cell Sci.* 113:1903–1912.

Johnston, M. 1999. Feasting, fasting and fermenting. Glucose sensing in yeast and other cells. *Trends Genet.* 15:29–33. http://dx.doi.org/10.1016/S0168-9525(98)01637-0

Kehat, I., F. Accornero, B.J. Aronow, and J.D. Molkentin. 2011. Modulation of chromatin position and gene expression by HDAC4 interaction with nucleoporins. *J. Cell Biol.* 193:21–29. http://dx.doi.org/10.1083/jcb.201101046

Kiermaier, E., S. Woehrer, Y. Peng, K. Mechtler, and S. Westermann. 2009. A Dam1-based artificial kinetochore is sufficient to promote chromosome segregation in budding yeast. *Nat. Cell Biol.* 11:1109–1115. http://dx.doi.org/10.1038/ncb1924

Köhler, A., M. Schneider, G.G. Cabal, U. Nehrbass, and E. Hurt. 2008. Yeast Ataxin-7 links histone deubiquitination with gene gating and mRNA export. *Nat. Cell Biol.* 10:707–715. http://dx.doi.org/10.1038/ncb1733

Koutelou, E., C.L. Hirsch, and S.Y. Dent. 2010. Multiple faces of the SAGA complex. *Curr. Opin. Cell Biol.* 22:374–382. http://dx.doi.org/10.1016/j.ceb.2010.03.005

Lee, T.I., H.C. Causton, F.C. Holstege, W.C. Shen, N. Hannett, E.G. Jennings, F. Winston, M.R. Green, and R.A. Young. 2000. Redundant roles for the TFIID and SAGA complexes in global transcription. *Nature.* 405:701–704. http://dx.doi.org/10.1038/35015104

Luthra, R., S.C. Kerr, M.T. Harreman, L.H. Apponi, M.B. Fasken, S. Ramineni, S. Chaurasia, S.R. Valentini, and A.H. Corbett. 2007. Actively transcribed GAL genes can be physically linked to the nuclear pore by the SAGA chromatin modifying complex. *J. Biol. Chem.* 282:3042–3049. http://dx.doi.org/10.1074/jbc.M608741200

Michaelis, C., R. Ciosk, and K. Nasmyth. 1997. Cohesins: chromosomal proteins that prevent premature separation of sister chromatids. *Cell.* 91:35–45. http://dx.doi.org/10.1016/S0092-8674(01)80007-6

Pijnappel, W.W., D. Schaft, A. Roguev, A. Shevchenko, H. Tekotte, M. Wilm, G. Rigaut, B. Séraphin, R. Aasland, and A.F. Stewart. 2001. The *S. cerevisiae* SET3 complex includes two histone deacetylases, Hos2 and Hst1, and is a meiotic-specific repressor of the sporulation gene program. *Genes Dev.* 15:2991–3004. http://dx.doi.org/10.1101/gad.207401

Pombo, A., and N. Dillon. 2015. Three-dimensional genome architecture: players and mechanisms. *Nat. Rev. Mol. Cell Biol.* 16:245–257. http://dx.doi.org/10.1038/nrm3965

Rodríguez-Navarro, S., T. Fischer, M.J. Luo, O. Antúnez, S. Brettschneider, J. Lechner, J.E. Pérez-Ortín, R. Reed, and E. Hurt. 2004. Sus1, a functional component of the SAGA histone acetylase complex and the nuclear pore-associated mRNA export machinery. *Cell.* 116:75–86. http://dx.doi.org/10.1016/S0092-8674(03)01025-0

Rohner, S., S.M. Gasser, and P. Meister. 2008. Modules for cloning-free chromatin tagging in *Saccharomyces cerevisae*. *Yeast.* 25:235–239. http://dx.doi.org/10.1002/yea.1580

Russel, D., K. Lasker, B. Webb, J. Velázquez-Muriel, E. Tjioe, D. Schneidman-Duhovny, B. Peterson, and A. Sali. 2012. Putting the pieces together: integrative modeling platform software for structure determination of macromolecular assemblies. *PLoS Biol.* 10:e1001244. http://dx.doi.org/10.1371/journal.pbio.1001244

Somech, R., S. Shaklai, O. Geller, N. Amariglio, A.J. Simon, G. Rechavi, and E.N. Gal-Yam. 2005. The nuclear-envelope protein and transcriptional repressor LAP2beta interacts with HDAC3 at the nuclear periphery, and induces histone H4 deacetylation. *J. Cell Sci.* 118:4017–4025. http://dx.doi.org/10.1242/jcs.02521

Taddei, A., C. Maison, D. Roche, and G. Almouzni. 2001. Reversible disruption of pericentric heterochromatin and centromere function by inhibiting deacetylases. *Nat. Cell Biol.* 3:114–120. http://dx.doi.org/10.1038/35055010

Taddei, A., F. Hediger, F.R. Neumann, C. Bauer, and S.M. Gasser. 2004. Separation of silencing from perinuclear anchoring functions in yeast Ku80, Sir4 and Esc1 proteins. *EMBO J.* 23:1301–1312. http://dx.doi.org/10.1038/sj.emboj.7600144

Taddei, A., G. Van Houwe, F. Hediger, V. Kalck, F. Cubizolles, H. Schober, and S.M. Gasser. 2006. Nuclear pore association confers optimal expression levels for an inducible yeast gene. *Nature.* 441:774–778. http://dx.doi.org/10.1038/nature04845

Therizols, P., T. Duong, B. Dujon, C. Zimmer, and E. Fabre. 2010. Chromosome arm length and nuclear constraints determine the dynamic relationship of yeast subtelomeres. *Proc. Natl. Acad. Sci. USA.* 107:2025–2030. http://dx.doi.org/10.1073/pnas.0914187107

Timney, B.L., J. Tetenbaum-Novatt, D.S. Agate, R. Williams, W. Zhang, B.T. Chait, and M.P. Rout. 2006. Simple kinetic relationships and nonspecific competition govern nuclear import rates in vivo. *J. Cell Biol.* 175:579–593. http://dx.doi.org/10.1083/jcb.200608141

Tjong, H., K. Gong, L. Chen, and F. Alber. 2012. Physical tethering and volume exclusion determine higher-order genome organization in budding yeast. *Genome Res.* 22:1295–1305. http://dx.doi.org/10.1101/gr.129437.111

Tong, A.H.Y., and C. Boone. 2007. 16 High-throughput strain construction and systematic synthetic lethal screening in *Saccharomyces cerevisiae*. *Methods Microbiol.* 36:369–386, 706–707. http://dx.doi.org/10.1016/S0580-9517(06)36016-3

Tong, A.H., M. Evangelista, A.B. Parsons, H. Xu, G.D. Bader, N. Pagé, M. Robinson, S. Raghibizadeh, C.W. Hogue, H. Bussey, et al. 2001. Systematic genetic analysis with ordered arrays of yeast deletion mutants. *Science.* 294:2364–2368. http://dx.doi.org/10.1126/science.1065810

Vodala, S., K.C. Abruzzi, and M. Rosbash. 2008. The nuclear exosome and adenylation regulate posttranscriptional tethering of yeast GAL genes to the nuclear periphery. *Mol. Cell.* 31:104–113. http://dx.doi.org/10.1016/j.molcel.2008.05.015

Winzeler, E.A., D.D. Shoemaker, A. Astromoff, H. Liang, K. Anderson, B. Andre, R. Bangham, R. Benito, J.D. Boeke, H. Bussey, et al. 1999. Functional characterization of the S. cerevisiae genome by gene deletion and parallel analysis. *Science.* 285:901–906. http://dx.doi.org/10.1126/science.285.5429.901

Wong, H., H. Marie-Nelly, S. Herbert, P. Carrivain, H. Blanc, R. Koszul, E. Fabre, and C. Zimmer. 2012. A predictive computational model of the dynamic 3D interphase yeast nucleus. *Curr. Biol.* 22:1881–1890. http://dx.doi.org/10.1016/j.cub.2012.07.069

Yang, X.J., and E. Seto. 2008. The Rpd3/Hda1 family of lysine deacetylases: from bacteria and yeast to mice and men. *Nat. Rev. Mol. Cell Biol.* 9:206–218. http://dx.doi.org/10.1038/nrm2346

Young, B.P., and C.J. Loewen. 2013. Balony: a software package for analysis of data generated by synthetic genetic array experiments. *BMC Bioinformatics.* 14:354. http://dx.doi.org/10.1186/1471-2105-14-354